CrossMark

# The influence of polyoxymethylene molar mass on the oxidative thermal degradation of its nanocomposites with hydroxyapatite

Kinga Pielichowska[1]

**Abstract** In this paper, the influence of mass-average molar mass ($M_w$) of polyoxymethylene (POM) copolymer on the thermooxidative degradation behavior of its nanocomposites with hydroxyapatite (HAp) is reported. POM copolymers' thermal stability slightly decreases with a decrease in mass-average molar mass. Thermal stability of POM/HAp nanocomposites is lower in comparison with pure POM, and it gets lower with a decrease in mass-average molar mass of POM copolymer. For POM copolymer with the highest molar mass, thermal stability of POM/HAp nanocomposite was ca. 30 °C lower than for pure POM. To get a more in-depth insight into the decomposition process, kinetic analysis of POM/HAp nanocomposite thermal degradation process was performed using Friedman, Ozawa–Flynn–Wall and multiple nonlinear regression methods. The best fit for pristine T2, T3 and T4 copolymers with different molar mass of 100768, 74727 and 68377 g mol$^{-1}$, respectively, was obtained for one-stage degradation mechanism with autocatalysis, while for T2/10 % HAp and T3/10 % it was parallel reaction model with autocatalysis (Bna) and phase-boundary reaction models (R3). For T4/10 % HAp, the best approximation was found for R2–Bna–D3 reaction model. From hyphenated TG–MS and TG–FTIR thermoanalytical studies, it was found that the main degradation product for POM/HAp nanocomposites is formaldehyde and the amount of other degradation products is lower in comparison with non-modified POM copolymers.

## Introduction

Polyoxymethylene (POM), also known as polyacetal, is a popular and attractive thermoplastic engineering polymer due to its properties of fatigue endurance, high stiffness, resistance to creep and low friction coefficient. It has a wide range of applications mainly in automotive, electrical and mechanical industry [1, 2]. However, POM is inherently unstable because its repeating oxymethylene units are usually terminated with thermally unstable hemi-formal terminals [3, 4]. POM tends to degrade from these unstable terminal groups by an 'unzipping' process, and in consequence, oxymethylene units are removed from the end of the chain one by one until the whole chain degrades. One of the main methods of improving thermal stability of POM is copolymerization with thermally stable monomers (e.g., ethylene oxide, dioxolane, dioxepane). Introduction of comonomer unit reduces the degradation sensitivity because the driving processes are decelerated and even stopped at the first comonomer unit [5]. However, these comonomer units strongly affect the thermal and chemical behavior of the copolymer. Thus, the properties of POM copolymers depend on the comonomer composition and on the sequence distribution (e.g., random or block) of the constituent comonomers [6].

POM copolymers are characterized by higher thermal stability, but their crystallinity degree is reduced in comparison with POM homopolymer. This is a result of lower carbon–carbon group interactions as these groups are separated in the macrochain. POM copolymer imparts superior

✉ Kinga Pielichowska
kingapie@agh.edu.pl

[1] Department of Biomaterials, Faculty of Materials Science and Ceramics, AGH University of Science and Technology, Al. Mickiewicza 30, 30-059 Kraków, Poland

Springer

resistance to alkali, hot water and other chemicals, longer life at elevated temperatures and more latitude in processing conditions [7], but its tensile strength, rigidity, softening and melting points are all lower than those found in POM homopolymer [8, 9].

Very little data are available on the influence of average molar mass of POM copolymer on its thermal stability. Kern and Cherdron [10] reported that with increasing average molar mass a faster degradation has to be expected for POM homopolymers. Five different reactions were postulated to occur at the initial stage of decomposition [10]: (1) depolymerization, starting on both ends of the polymer chain, (2) autooxidative fission, (3) decomposition by secondary products of the polymer chain, (4) thermal degradation and (5) hydrolysis and acidolysis. Initiation steps are followed by a chain scission with formaldehyde formation. The degradation rate of chain scission is higher than that of the initial step; in chains with higher molar mass, more formaldehyde formation occurs and the degradation rate increases linearly with increasing molar mass. On the other hand, Pan et al. [6] postulated that the degradation process of POM copolymer could be divided into three stages with a gradually increasing degradation rate: (1) At the beginning, POM chain tends to split off formaldehyde, starting at the chain ends, some of which were not ended by ethylene oxide (EO) units; (2) in the second stage, the thermooxidation of POM takes place in the amorphous phase, and finally, in the last stage, further random chain scission and unzipping occur in the crystalline phase. In the work done by Archodoulaki et al. [11], it was found that the onset temperature of degradation for POM copolymer with the highest average molar mass was the highest.

Similar trend was observed in our previous work [12]. Additionally, significant influence of HAp nanoparticles on the thermal stability of POM copolymer was observed—for nanocomposites with 10 mass% of HAp, thermal stability decreased by 33 °C for POM with $M_w = 100768$ g mol$^{-1}$ and 59 °C for POM with $M_w = 68377$ g mol$^{-1}$. These results can suggest that the influence of HAp on the thermal stability of POM matrix strongly depends on the POM mass-average molar mass. Thus, in this study, the influence of mass-average molar mass of POM on the thermooxidative degradation behavior of POM and its nanocomposites with hydroxyapatite (HAp) is reported.
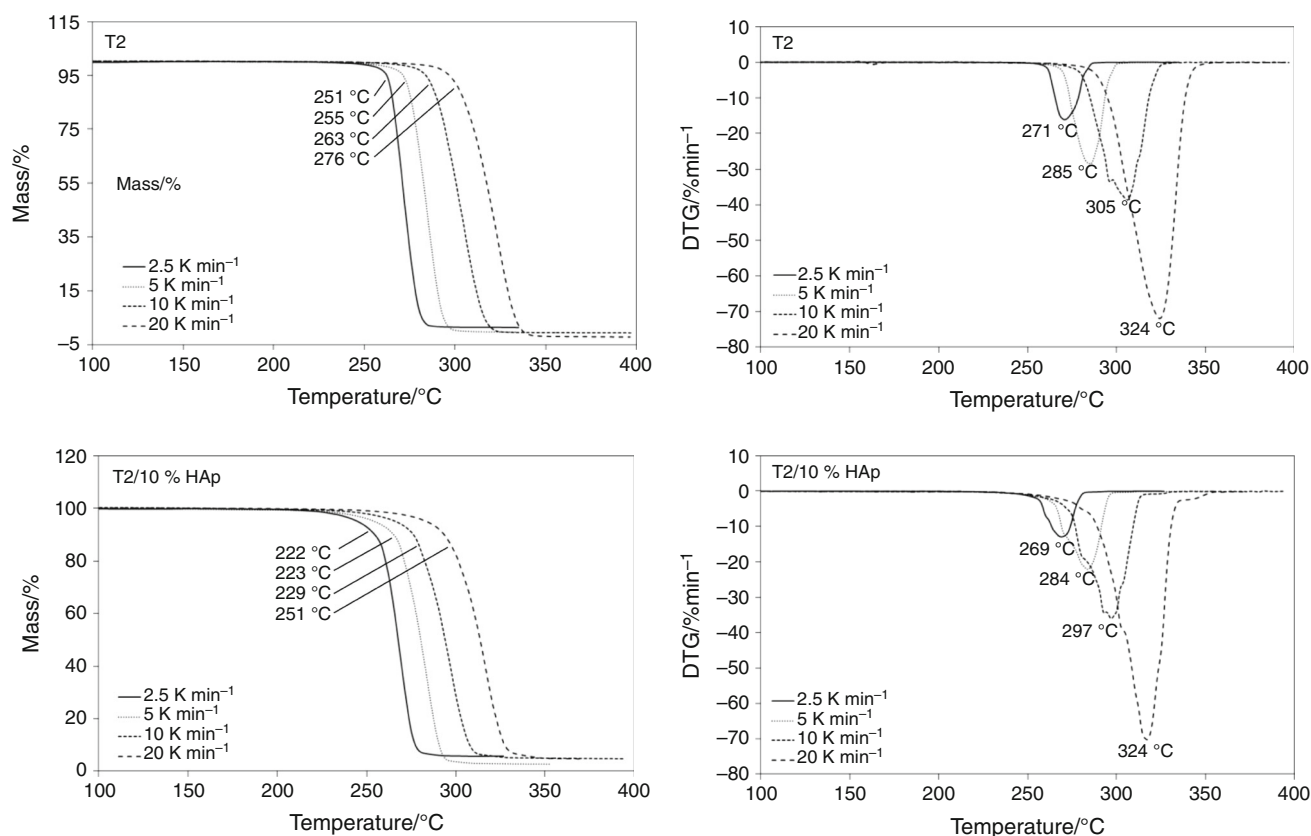


Fig. 1 TG (*left*) with temperatures corresponding to 1 % mass loss and DTG (*right*) profiles of T2 and T2/10 % HAp nanocomposites at different heating rates of 2.5, 5, 10 and 20 K min$^{-1}$

# Experimental

## Materials and preparation

Three commercial grades of POM copolymer T200 (T2), T300 (T3) and T411 (T4) (Tarnoform®) with melt flow rate (MFR 190/2.16, ISO 1133) of 2.5, 9.0 and 13 g/10 min, respectively, were supplied by Z.A. Tarnów-Mościce SA. Molar mass was determined by GPC at 40 °C on a VE2001 Viscotek GPC System with a RI–VE 3580 (Viscotek) detector, using a PL HFIP gel, 605 E901506 and HFIP 603 E910606 columns. Average molar masses (based on polystyrene standard) were determined as: $M_n = 9368$ g mol$^{-1}$ and $M_w = 100768$ g mol$^{-1}$, $M_w/M_n = 10.76$ for T2, $M_n = 8614$ g mol$^{-1}$ and $M_w = 74727$ g mol$^{-1}$, $M_w/M_n = 8.67$ for T3 and $M_n = 10203$ g mol$^{-1}$, $M_w = 68377$ g mol$^{-1}$, $M_w/M_n = 6.70$ for T4. Hydroxyapatite $Ca_{10}(PO_4)_6OH_2$ nanopowder with a nanoparticle size below 100 nm (99 % of particles) was product of nGimat Co. (Atlanta, USA).

POM and POM/HAp nanocomposites were prepared by melt processing method. Firstly, POM and HAp were airdried in a laboratory drier for 4 h at 50 °C, then mechanically mixed at room temperature to get homogeneous mixture (0 and 10.0 % w/w of HAp) and again dried for 1 h at 50 °C. Next, pristine POM and POM/HAp blends were put into sealed polyethylene bags to avoid contact with moisture. The dry materials were extruded in a double-screw extruder (ThermoHaake PolyLab PTW 16/25) at a rotary speed of 50 rpm. The temperature profiles of the barrel were as follows: for T2 185–190–190–190 °C, for T3 185–190–190–185 °C and for T4 190–190–190–185 °C. Compositions were shaped by using a DSM laboratory injection molding machine.

## Techniques

### Thermogravimetric analysis

Thermogravimetric analysis was performed using a Netzsch TG 209 thermal analyzer, operating in a dynamic mode at a heating rate of 2.5, 5, 10 and 20 K min$^{-1}$. The conditions were sample mass ca. 5 mg, and each sample has similar cuboid shape taken always from the same place from specimens after injection molding. Measurements were taken in air atmosphere with air flow rate 30 cm$^3$ min$^{-1}$ in an open α-$Al_2O_3$ pan. The raw data were converted to ASCII files, and kinetic analysis was carried
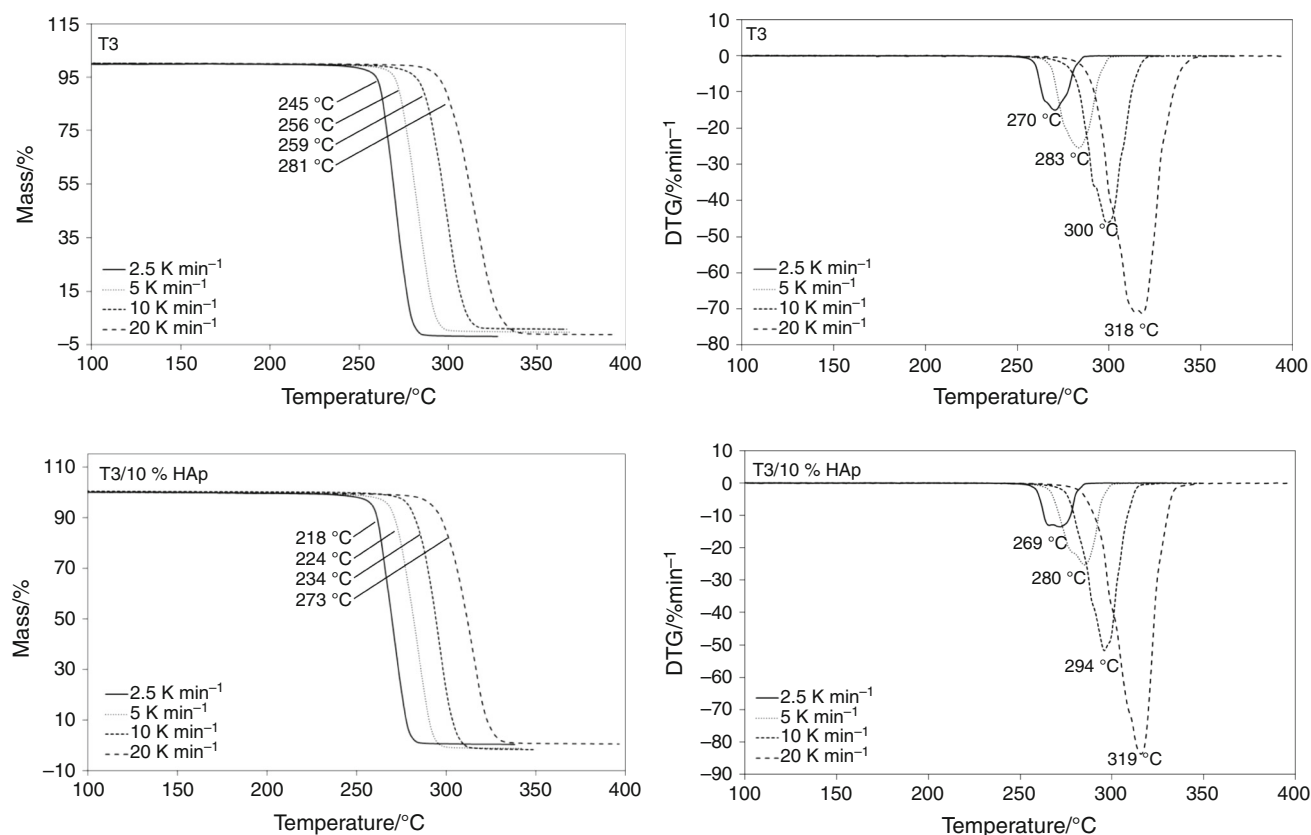


Fig. 2 TG (*left*) with temperatures corresponding to 1 % mass loss and DTG (*right*) profiles of T3 and T3/10 % HAp nanocomposites at different heating rates: 2.5, 5, 10 and 20 K min$^{-1}$

out using an in-house program and a Netzsch Thermokinetic Program (v. 99/10).

## Thermogravimetric analysis coupled with Fourier transform infrared spectroscopy

Thermogravimetric analysis coupled with Fourier transform infrared spectroscopy (TG/FTIR) was carried out using a Mettler-Toledo TGA/SDTA 851 thermal analyzer

(heating rate 10 K min$^{-1}$, sample mass 5 mg, air flow 50 cm$^3$ min$^{-1}$) and a JASCO 610 FTIR spectrometer with resolution of 2 cm$^{-1}$.

## Thermogravimetric analysis coupled with mass spectroscopy

Thermogravimetric analysis coupled with mass spectroscopy (TG/MS) was performed with a TA Instruments
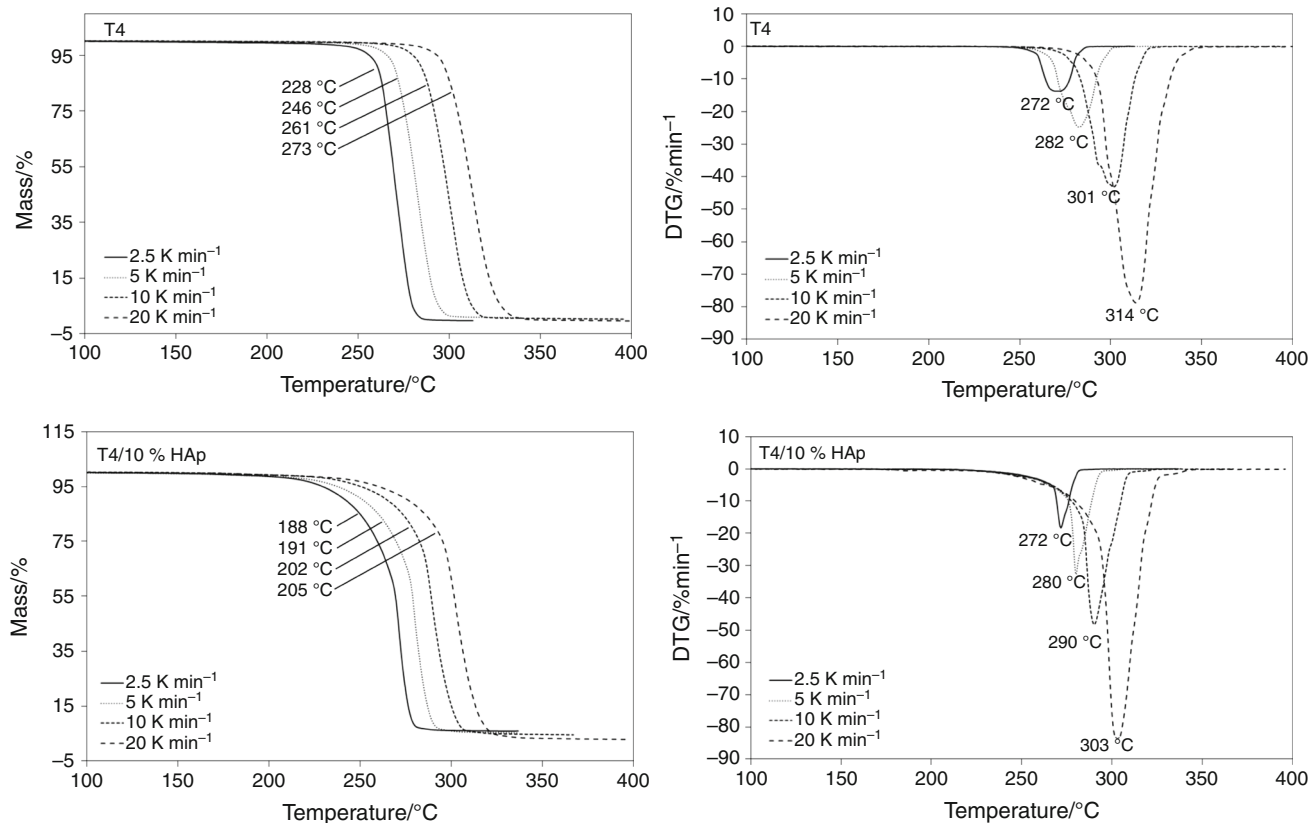


Fig. 3 TG (*left*) with temperatures corresponding to 1 % mass loss and DTG (*right*) profiles of T4 and T4/10 % HAp nanocomposites at different heating rates: 2.5, 5, 10 and 20 K min$^{-1}$

**Table 1** Kinetic models [19–22]

| Model | f(α) | Symbol |
|---|---|---|
| Reaction first order | $(1 - \alpha)$ | F1 |
| Reaction second order | $(1 - \alpha)^2$ | F2 |
| Reaction of nth order | $(1 - \alpha)^n$ | Fn |
| Phase-boundary-controlled reaction (contracting area) | $(1 - \alpha)^{1/2}$ | R2 |
| Phase-boundary-controlled reaction (contracting volume) | $(1 - \alpha)^{2/3}$ | R3 |
| Prout–Tompkins equation | $(1 - \alpha)^n \alpha^a$ | Bna |
| Reaction of first order with autocatalysis | $(1 - \alpha)(1 + J_{kat.}\alpha)$ | C1 |
| Reaction of nth order with autocatalysis | $(1 - \alpha)^n(1 + J_{kat.}\alpha)$ | Cn |
| Two-dimensional growth of nuclei (Avrami equation) | $2[-\ln(1 - \alpha)^{1/2}](1 - \alpha)$ | A2 |
| Three-dimensional growth of nuclei (Avrami equation) | $3[-\ln(1 - \alpha)^{2/3}](1 - \alpha)$ | A3 |
| n-Dimensional nucleation (Avrami–Erofeev equation) | $n[-\ln(1 - \alpha)^n](1 - \alpha)$ | An |

2960 SDT thermal analyzer (heating rate 20 K min$^{-1}$, sample mass 5 mg, air flow = 100 cm$^3$ min$^{-1}$) and a Balzers Thermo-Star quadrupole mass spectrometer. The ionizing voltage of the crossbeam electron impact ionization source was 70 eV. The thermogravimetric analyzer and spectrometer were suitably coupled to enable the passage of evolved products from the furnace to the gas cell over a short heated path, to minimize secondary reaction or condensation on cell walls.

## Results and discussion

In our previous study [12], it was found that with an increase in HAp nanoparticles' content in POM nanocomposites, the thermal stability of POM decreases and the most profound effect was observed for the material containing 10 mass% of HAp. Therefore, detailed kinetic and thermoanalytical studies were planned in the course of this work for POM copolymers of different molar mass with 10 % of HAp content. It has been found that in T4/HAp nanocomposite a major decrease in the thermal stability in TG experiment of ca. 59 °C occurred, and in T2/HAp and T3, the thermal stability was lowered by ca. 30 °C. TG and DTG curves at different heating rates of T2, T3 and T4 POM copolymers, as well as POM/HAp nanocomposites, are presented in Figs. 1–3, respectively. Please note that the TG profile and data of POM and POM/HAp nanocomposites obtained at the heating rate of 10 K min$^{-1}$ have already been presented in Ref. [12].

It can be seen that the onset of decomposition temperature on TG/DTG profiles taken at the heating rate of 10 K min$^{-1}$ is ca. 263, 259 and 261 for T2, T3 and T4 copolymers, respectively [12], while for nanocomposites with 10 mass% of nanohydroxyapatite it is ca. 229 °C for T2/HAp, 234 °C for T3/HAp and 202 °C for T4/HAp
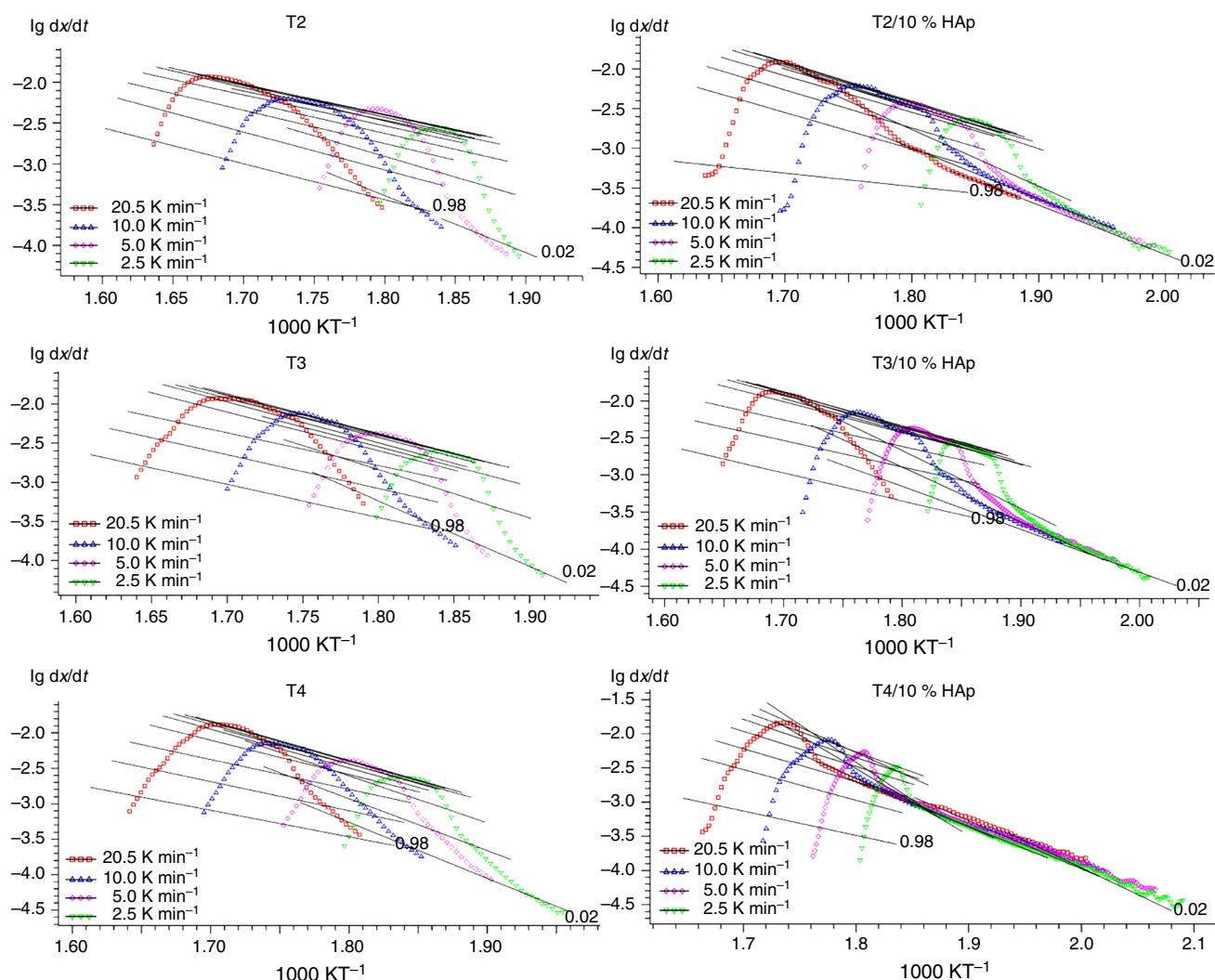


Fig. 4 Friedman analysis of the thermal degradation of POM and POM/HAp nanocomposites

composites. The decomposition seems to proceed in a single step, but DTG profiles for pristine T2, T3 and T4 POM reveal the occurrence of at least two overlapping peaks. For nanocomposites with HAp, minor influence on thermal degradation can be seen for those based on T2 and T3 copolymers; however, three overlapping peaks can be detected. The influence of HAp on the thermal decomposition of POM is much more visible for T4 copolymer—in both TG and DTG profiles, remarkable shape changes can be observed that suggest the relation between the HAp action on POM copolymer matrix and its mass-average molar mass.

Due to its chemical structure and composition, HAp can act as a catalyst in numerous reactions of organic compounds such as oxidation reaction (oxidation of alcohols and dehydrogenations of hydrocarbons), reduction reaction

(hydrogenolysis and hydrogenation) and the formation of C–C bonds (Claisen–Schmidt condensation reaction, Michael addition reaction, Knoevenagel condensation reaction, Fridel–Crafts reaction, Heck reaction, Diels–Alder and aldol reactions) [13–15]. In spite of the broad application of HAp as a (nano) filler for different polymer matrices, especially for biomedical applications [16, 17], there are little data on the influence of HAp on the degradation mechanisms and stability of macromolecular compounds.

It was observed during processing that introduction of HAp nanoparticles in amount of 10 % into POM (both homopolymer and copolymer) matrix leads to significant decrease in thermal stability of POM. Kinetics of this process may be analyzed using isoconversional methods (Friedman method and Ozawa–Flynn–Wall method), and
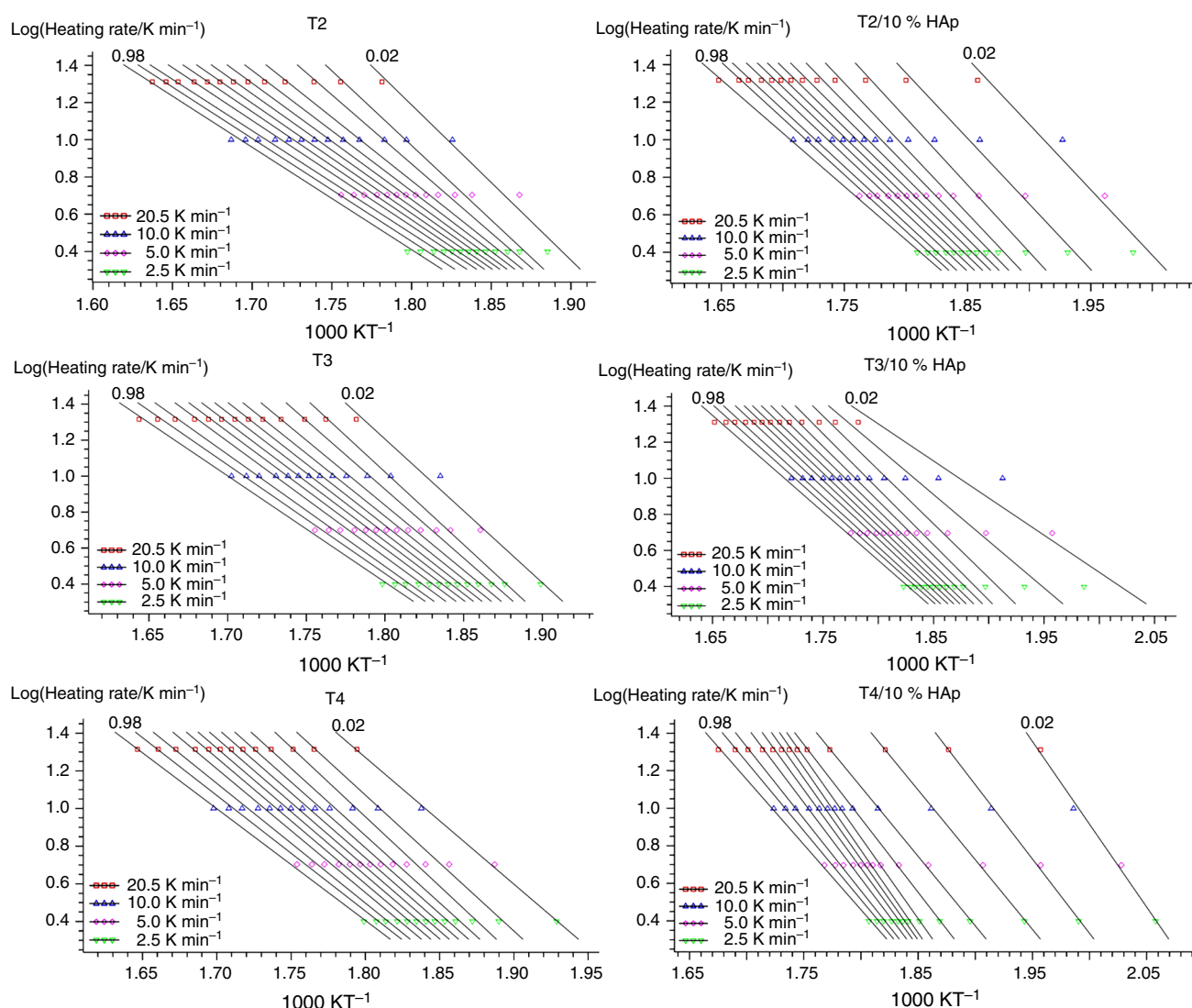


Fig. 5 Ozawa–Flynn–Wall analysis of the thermal degradation of POM and POM/HAp nanocomposites

multiple nonlinear regression method was applied according to the procedure described in [18, 19]. The most frequently used mathematical models to describe thermal degradation of polymers used in this work are presented in Table 1 [19–22].

Hence, graphical results of Friedman and Ozawa–Flynn–Wall analyses are presented in Figs. 4 and 5, while activation energy diagrams for both methods are presented in Fig. 6.

Generally, Friedman plots for pristine T2, T3 and T4 copolymers look similar and only one maximum can be observed. The slope of experimental points fit is higher than the slope of Friedman lines for the curves that have been calculated from measurements in relation to the isoconversional lines. These results suggest that degradation of POM run in one main stage and that the starting reaction is autocatalytically activated [23].

For T2/10 % HAp and T3/10 % HAp composites, the slope of experimental points is lower than for pristine T2 and T3, but still it is higher than the slope of Friedman lines which suggest an autocatalytically activated process. Additionally, based on our previous findings [18], we assumed that reaction of POM degradation partially undergoes in (1) POM bulk with autocatalytic mechanism as for pristine POM, and (2) on the phase-boundary POM–HAp. For T4/10 % HAp, some changes can be observed in comparison with T2/10 % HAp and T3/10 % HAp systems—on the beginning, the slope of experimental points is lower than isoconversional lines, and then, maximum with a higher slope than the slope of Friedman lines is detected. It suggests that the thermal degradation process of T4/10 % HAp composite goes through at least two or three stages and one of the reactions is phase-boundary processes or $n$th-order process. However, due to release of large amounts of formaldehyde, one can expect that diffusion-controlled processes may take place, too. In the Ozawa–Flynn–Wall plots, changes in the slope of isoconversional lines indicate complex mechanism of degradation and changes in activation energy versus degree of conversion [24]. The diagrams for the latter function, determined by the Friedman and Ozawa–Flynn–Wall methods, display a similar large maximum at $\alpha = 0.4$–$0.5$. For pristine T2, T3 and T4 copolymers and T2/10 % HAp and T3/10 % HAp nanocomposites, activation energy of thermal degradation process seems to be constant that suggests a one-step degradation process.

In the next stage, the multiple nonlinear regression method was employed to fit the model for $f(\alpha)$ function to the profile of the experimental TG curve. It was assumed that the thermal degradation process of POM is catalyzed on the phase boundary with HAp nanoparticles, and POM macrochains degrade autocatalytically by chain scission.
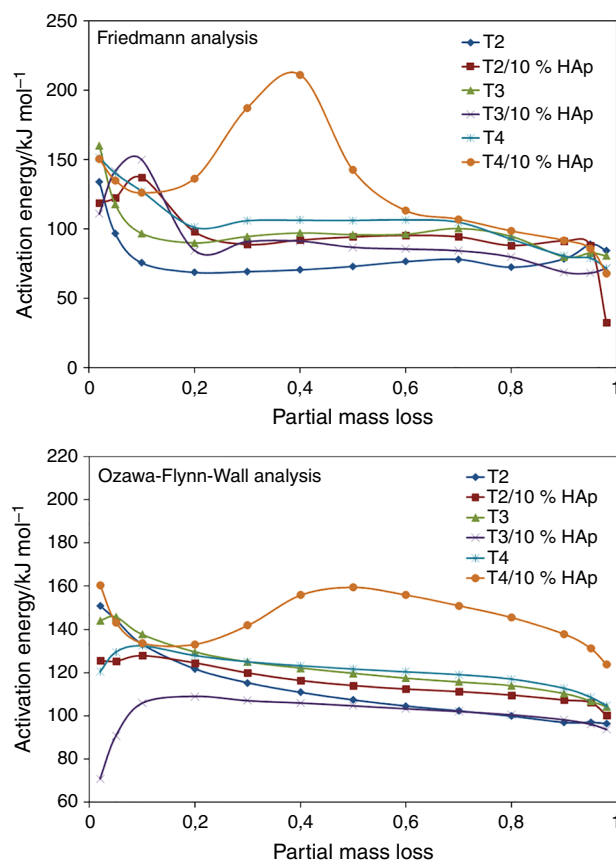


**Fig. 6** Calculated values of the activation energy from the Friedman and Ozawa–Flynn–Wall analyses of the degradation process of POM and POM/HAp nanocomposites

The degree of matching was determined with the use of $F$ test and correlation coefficient. The results of calculations using multiple nonlinear regression method are presented in Table 2 and Fig. 7.

For pristine T2, T3 and T4 POM copolymers, the best fit between the experimental data and mathematical models was obtained for one-stage degradation mechanism with autocatalysis. These results stay with good agreement with isoconversion studies for T2, T3 and T4 copolymers based on Friedman method, where autocatalytic nature of the POM degradation process was suggested. Generally, autocatalysis occurs when the products catalyze the reaction; reactants are regenerated during a reaction [25]. During POM degradation, the evolved formaldehyde autocatalyzes the decomposition process of POM. Values of the calculated activation energy are ca. 108, 119 and 121 kJ mol$^{-1}$ for T2, T3 and T4 copolymers, respectively, and they are in similar range as calculated by Ozawa–Flynn–Wall method. In all three methods, the lowest activation energy for degradation process was observed for T2 copolymer which was characterized by the highest $M_w$,

**Table 2** Results of nonlinear regression

| Sample | Reaction model | $E_{a1}$/ kJmol⁻¹ | Stand. dev. | log$A_1$ | Stand. dev. | Model | $E_{a2}$/ kJmol⁻¹ | Stand. dev. | log$A_2$ | Stand. dev. | Model | $E_{a3}$/ kJmol⁻¹ | Stand. dev. | log$A_3$ | Stand. dev. | Model | F-test | Corr. coeff. |
|---|---|---|---|---|---|---|---|---|---|---|---|---|---|---|---|---|---|---|
| | | **1** | | | | | **2** | | | | | **3** | | | | | | |
| T200 | A →1→ B | 107.5 | 0.7 | 8.27 | 0.07 | Bna | | | | | | | | | | | 1.000 | 0.999 |
| | A →1→ B | 108.1 | 0.8 | 6.13 | 0.09 | CnB | | | | | | | | | | | 1.017 | 0.999 |
| | A →1→ B | 107.5 | 0.7 | 6.25 | 0.07 | C1B | | | | | | | | | | | 1.083 | 0.999 |
| T200/ 10% HAp | A →1→ B, →2→ C | 136.0 | 3.3 | 9.31 | 0.30 | R3 | 95.2 | 2.6 | 7.23 | 0.22 | Bna | | | | | | 1.000 | 0.999 |
| | A →1→ B, →2→ C | 135.0 | 3.3 | 9.39 | 0.31 | R2 | 95.0 | 2.9 | 7.24 | 0.24 | Bna | | | | | | 1.010 | 0.999 |
| | A →1→ B, →2→ C | 136.8 | 5.4 | 9.22 | 0.53 | R3 | 102.1 | 4.0 | 3.20 | 0.15 | CnB | | | | | | 1.048 | 0.999 |
| T300 | A →1→ B | 119.4 | 0.5 | 9.40 | 0.06 | Bna | | | | | | | | | | | 1.000 | 0.999 |
| | A →1→ B | 119.3 | 0.6 | 7.30 | 0.07 | CnB | | | | | | | | | | | 1.078 | 0.999 |
| | A →1→ B | 118.8 | 0.6 | 8.69 | 0.05 | An | | | | | | | | | | | 1.341 | 0.999 |
| T300/ 10% HAp | A →1→ B, →2→ C | 121.0 | 7.4 | 7.61 | 0.69 | R3 | 99.0 | 3.5 | 7.67 | 0.32 | Bna | | | | | | 1.000 | 0.997 |
| | A →1→ B, →2→ C | 119.9 | 7.6 | 7.68 | 0.71 | R2 | 99.5 | 3.6 | 7.71 | 0.33 | Bna | | | | | | 1.002 | 0.997 |
| | A →1→ B, →2→ C | 120.1 | 10.6 | 7.36 | 1.03 | R3 | 101.6 | 3.9 | 3.02 | 0.64 | CnB | | | | | | 1.006 | 0.997 |
| T411 | A →1→ B | 121.2 | 0.6 | 9.52 | 0.06 | Bna | | | | | | | | | | | 1.000 | 0.999 |
| | A →1→ B | 121.2 | 0.6 | 7.65 | 0.06 | CnB | | | | | | | | | | | 1.008 | 0.999 |
| | A →1→ B | 120.9 | 0.6 | 8.90 | 0.06 | An | | | | | | | | | | | 1.187 | 0.999 |
| T411/ 10% HAp | A →1→ B, →2→ C, →3→ D | 149.9 | 3.9 | 10.94 | 0.44 | R2 | 99.9 | 10.9 | 9.46 | 0.58 | Bna | 214.8 | 12.6 | 15.81 | 1.05 | D3 | 1.000 | 0.999 |
| | A →1→ B, →2→ C, →3→ D | 149.9 | 3.9 | 10.60 | 0.43 | R3 | 99.5 | 10.9 | 9.04 | 0.57 | Bna | 204.0 | 12.5 | 14.84 | 1.01 | D4 | 1.153 | 0.999 |
| | A →1→ B, →2→ C, →3→ D | 149.9 | 3.2 | 10.95 | 0.36 | R3 | 99.8 | 13.3 | 9.69 | 0.58 | Bna | 176.6 | 23.0 | 11.97 | 1.90 | D3 | 1.533 | 0.999 |

while the highest activation energy was found for T4 POM with the lowest $M_w$.

T2 copolymer is characterized by the highest average molar mass, the lowest crystallinity and the lowest content of end-groups, while T4 copolymer has the lowest average molar mass, the highest crystallinity and the highest content of end-groups. As it was described in the literature, an increase in the activation energy can be attributed to the higher degree of crystallinity of T4 copolymer [26] manifested by better arrangement of polymer chains even in the molten state. More crystalline polymers require higher energy inputs to overcome their inter- and intramolecular forces, and the activation energy barrier is at higher level [27]. On the other hand, the highest viscosity of T2 melt can hinder diffusion, heat transport and, in consequence, increase thermal stability of POM. Enhancements in the thermal stability versus molar mass were also observed for other polymers [28]. Additionally, in the work by Archodulaki et al. [11], it was found that with an increase

in melt flow rate temperature for a mass loss of 3 % decreased.

As it can be seen, the pre-exponential factor increases with a decrease in mass-average molar mass of neat POM. The value of pre-exponential factor suggests that surface decomposition where the activated complex is highly restricted in rotation takes place. For POM/HAp nanocomposites, results for T2/10 % HAp and T3/10 % HAp look similar. The highest values of pre-exponential factor can be observed for T4/10 % HAp even up to ca. 16 that suggest bulk degradation with no change in the degree of rotational excitation between the reactants and the complex with completely restricted rotation [29]. This confirms our supposition that after introduction of HAp nanoparticles, HAp acts as a catalyst for thermal decomposition of POM matrix; this effect is particularly well visible for POM with the lowest molar mass.

For the POM composites with 10 mass% of HAp, it can be observed that effect of HAp nanoparticles on the
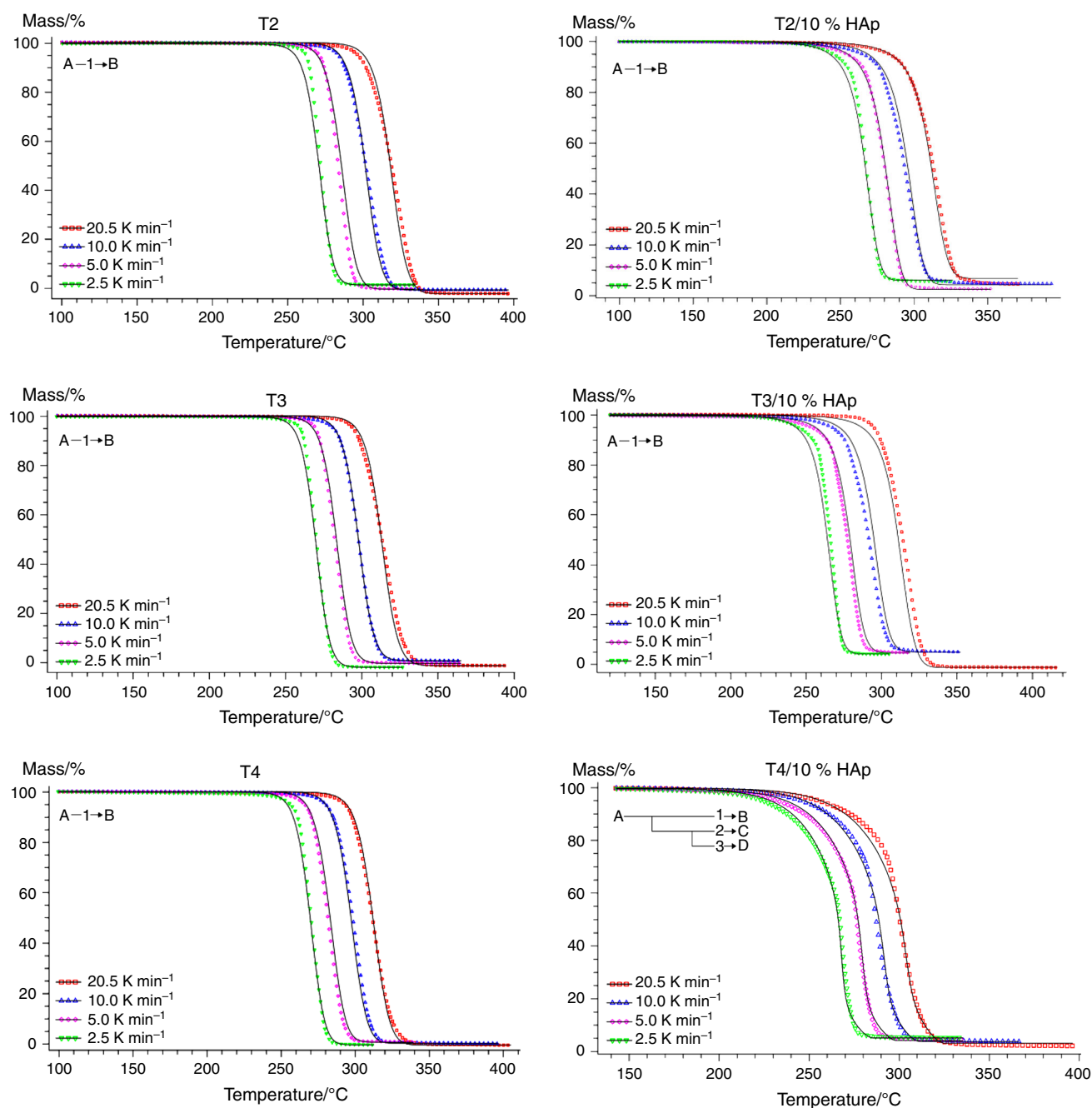
**Fig. 7** Best fit of kinetic model of the thermal decomposition process of T2, T3 and T4 as well T2/10 % HAp, T3/10 % HAp and T4/10 % HAp nanocomposites

kinetics of degradation of POM matrix strongly depends on mass-average polymer molar mass. For T2/10 % HAp and T3/10 % kinetic analysis, one assumed based on results of Friedman analysis parallel reaction model with autocatalysis and phase-boundary reaction. For both materials, the best fit was found for Bna and R3 (or R2) reaction models. R-type reaction models assume that reaction occurs rapidly on the surface of the particles—in R2 model, particle is cylindrical solid, while in R3 model particle is in spherical

or cubical shape [25, 30]. A thin surface layer of the product is located on the particle surface; chemical reaction is a rate-controlling process (so-called surface-controlled reaction), and the reaction rate is the proportional to surface area of the still unreacted particles [30]. It should be noted that lower activation energy for POM degradation with autocatalysis model for T2/10 % HAp and T3/10 % HAp composites in comparison with T2 and T3 copolymers was found. This effect can be attributed to the
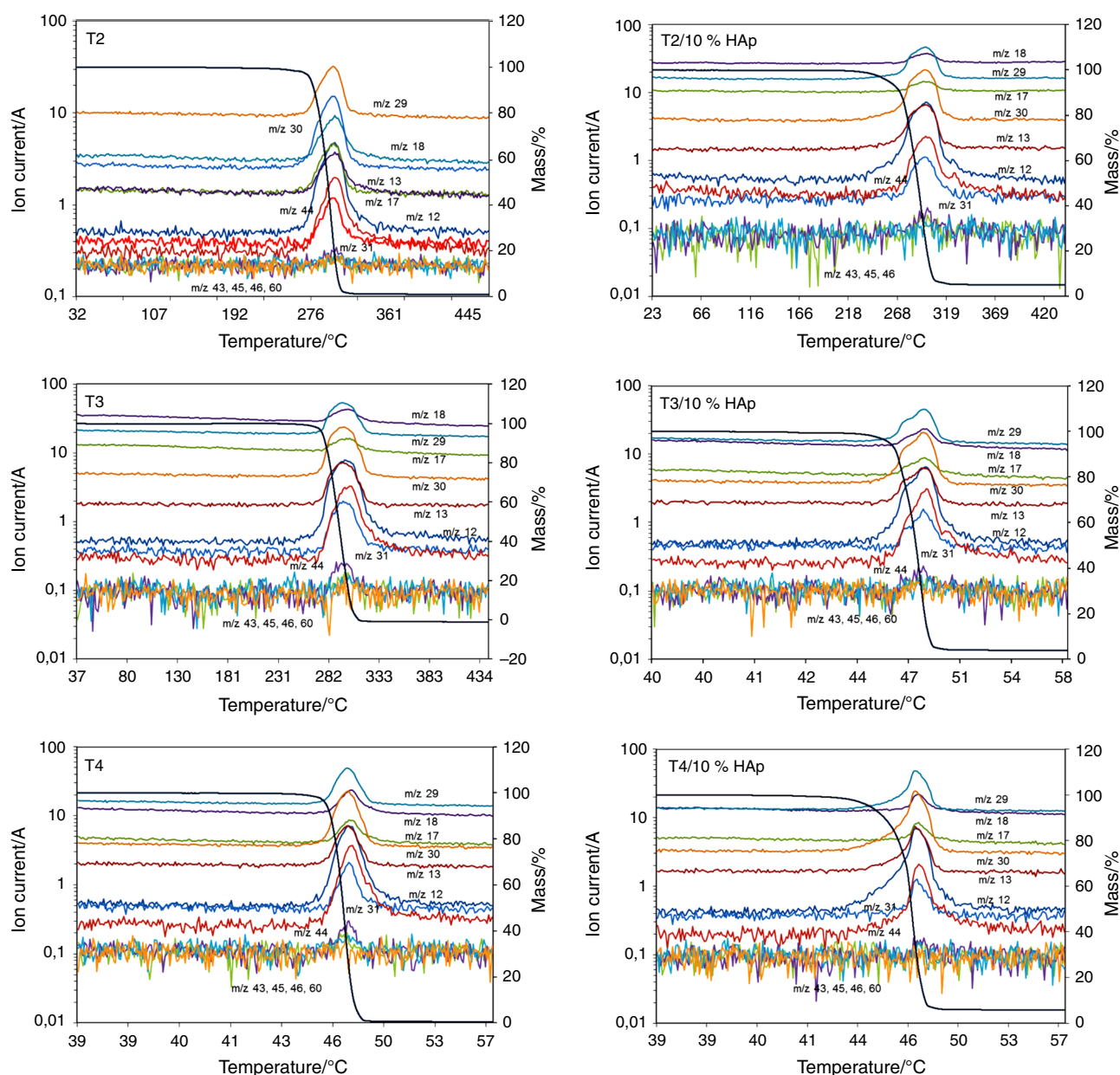
**Fig. 8** Intensity of evolution of selected volatile products formed during the thermal degradation of POM and POM/HAp nanocomposites

catalytic influence of HAp and formaldehyde which formation is accelerated by HAp presence, on POM degradation process [31–33].

As it was already found, in POM/HAp nanocomposite degradation process, formaldehyde is formed in much lower temperature than during virgin POM decomposition where only depolymerization process takes place. For T4/10 % HAp material, a third parallel diffusion-controlled reaction model was implemented into the calculation procedure. The reason was that during processing of this composition, rapid swelling of the polymer melt was observed connected to the rapid release and diffusion of

formaldehyde in the whole volume of the sample. In the nonlinear regression, the best fit was found for R2–Bna–D3 model and similar like for T2/10 % HAp and T3/10 %HAp composites activation energy for autocatalytic POM degradation was lower than for pure POM. The highest activation energy was found for D3 reaction model (over 200 kJ mol$^{-1}$), and it can explain higher activation energy of POM degradation process in T4/10 % HAp nanocomposite calculated by Friedman and Ozawa–Flynn–Wall methods. In diffusion-controlled processes, mass transport becomes rate-controlling factor and the main process is the gradual growth of the product layer. The vastly used Jander
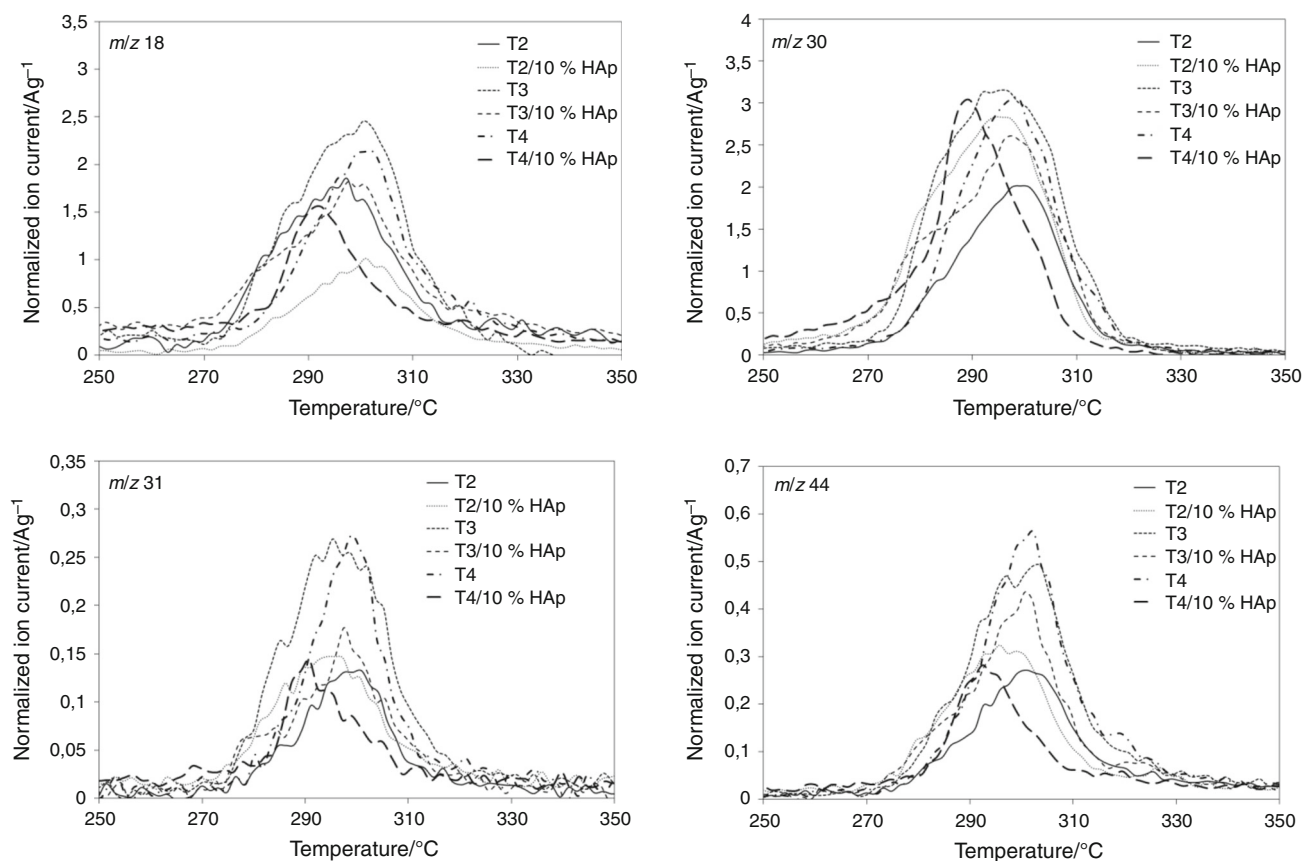
**Fig. 9** Normalized ion currents versus temperature for POM and POM/HAp nanocomposites

model (D3) of three-dimensional diffusion assumes that solid particles are of spherical shape [34] and parabolic law was applied to describe solid-state reactions. D4 three-dimensional model was proposed by Ginstling and Brounshtein [35] who replaced parabolic law by a dependence relating the growth of the product layer to the particle surface area [25, 30]. We suppose that during heating T4/10 % HAp composite undergoes degradation catalyzed by HAp in the whole volume with intensive emission of formaldehyde. Formaldehyde can easily evaporate from the surface, but from the bulk migration is strongly hindered, which leads to swelling of the sample observed during processing. The largest effect of samples swelling and formaldehyde odor was observed for T4/10 % HAp. Based on our observations, we can suspect that an increase in activation energy for T4/10 % HAp at partial mass loss 0.4–0.6 can be attributed to the most intensive diffusion of formaldehyde.

In the next stage, thermoanalytical studies were performed by using TG–MS and TG–FTIR coupled methods which make it possible to analyze online the volatile decomposition products and to get additional insight into degradation mechanism. Results of TG–MS measurements are presented in Fig. 8.

Several fragmentation ions formed during the thermal degradation of POM were detected in TG–MS measurements: $m/z$ 17 (–OH), $m/z$ 18 (water), $m/z$ 29 (fragment of $H_2C=O$ and other components), $m/z$ 30 (formaldehyde), $m/z$ 31 (fragment of $CH_3$-OH and trioxane) and $m/z$ 44 (carbon dioxide). No peaks for ions $m/z$ 43 (acetaldehyde), 45, 46 (formic acid), and 60 (acetic acid, methyl formate) were found. However, formic acid is rarely found, because formaldehyde is difficult to be oxidized to formic acid in the absence of oxygen. Formic acid found during degradation of commercial POM was more likely attributed to the processing additives [36]. In our case, degradation takes place in air atmosphere; however, it seems that only surface of the material is in contact with oxygen from air. The rest of the sample degrades without oxygen presence. We observed this effect on laboratory scale, when POM/HAp nanocomposites heated above the melting point of POM swollen due to rapid formation of formaldehyde inside the sample.

Different shapes of evolution profiles of main degradation products can be observed for POM samples and POM/HAp nanocomposites. Generally, for all POM samples, one broad peak for all degradation products can be observed, while for POM/HAp nanocomposites shape of peaks suggests two or
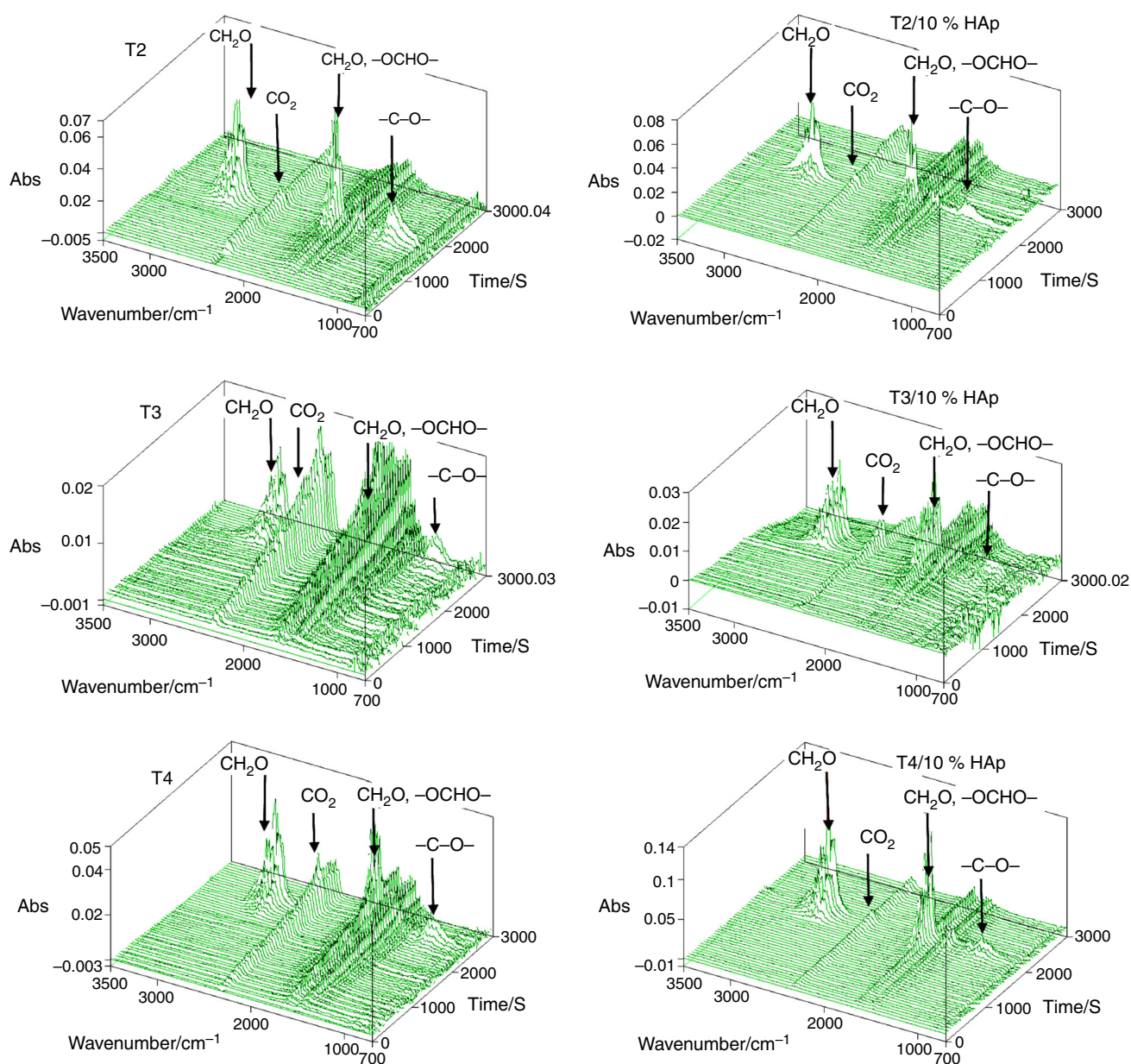
**Fig. 10** Stacked plots of IR spectra of volatile products evolved during the thermal degradation of POM and POM/HAp nanocomposites

three overlapping peaks for $m/z$ 29 and 30 and for other degradation product such as methanol ($m/z$ 31), $CO_2$ ($m/z$ 44) and $H_2O$ ($m/z$ 18). Additionally, the formic acid can be oxidized to water and carbon dioxide [8, 37, 38]. The limited amount of methanol ($CH_3OH$) may be related to the acidolysis and hydrolysis [36]. Peak $m/z$ 44 could also correspond to carbonyl, carboxyl or hydroperoxide groups formed in the main chain during thermooxidative degradation [8, 37, 39] which can induce chain scission followed by the formation of formaldehyde, but they can also oxidize the latter to formic acid. The both reactions are responsible for acidolytic degradation of the polyacetal chain [5].

Normalized ion currents versus temperature for POM and POM/HAp nanocomposites are presented in Fig. 9.

It can be observed that generally the highest amount of water ($m/z$ 18), methanol ($m/z$ 31) and carbon dioxide ($m/z$ 44) was formed for neat POM, while the largest emission of formaldehyde was observed for POM/HAp nanocomposites, especially for T3/10 % HAp and T4/10 % HAp, and also for neat T3 and T4. These results suggest that incorporation of HAp nanoparticles leads to a decrease in the amount of degradation products other than formaldehyde in comparison with neat POM, while the amount of emitted formaldehyde depends on the $M_w$ of POM.
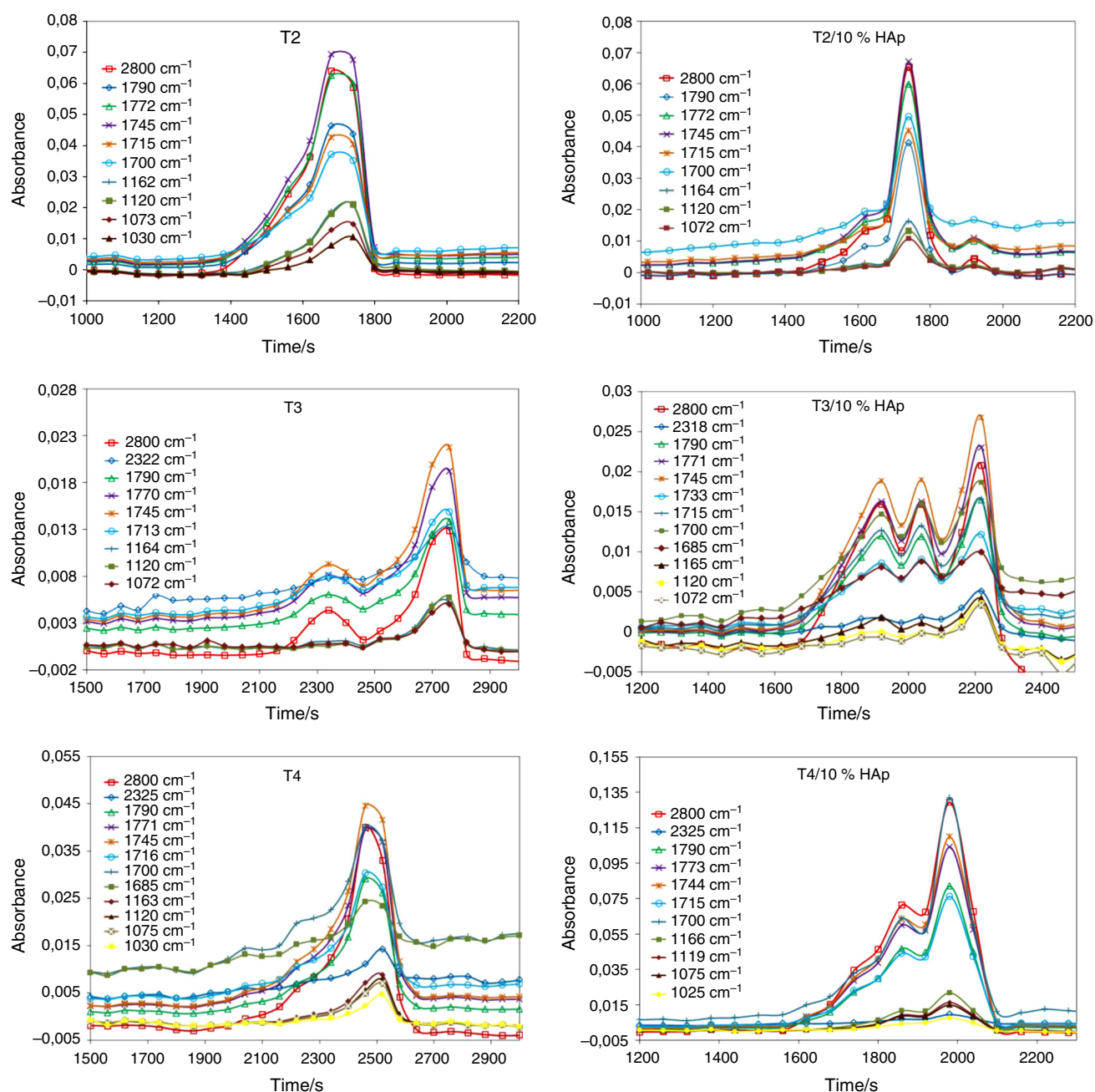
**Fig. 11** Intensity of characteristic absorption bands of thermal degradation products of POM and POM/HAp nanocomposites

TG–MS results can be nicely completed by TG–FTIR data—Fig. 10.

Based on the literature data, there are several characteristic absorption bands of volatiles evolved during the thermal degradation of POM: at ca. 1030 cm$^{-1}$ (C=O in aldehydes or carbon monoxide), at 1073, 1120, 1162 cm$^{-1}$ ($v$C–O in ethers and esters), at 1209 cm$^{-1}$ ($v$C–O for acids), at 1745 cm$^{-1}$ ($v$C=O in aldehydes), at 1755 cm$^{-1}$ ($v$C=O in esters or acids), and at 2800 cm$^{-1}$ (CH$_2$ in aldehydes) [36]. The main degradation products of T2, T3 and T4 copolymers are formaldehyde, carbon dioxide (which comes from the depolymerization of chain ends and random chain scission of oxymethylene chain), and, in smaller amounts, formic acid, acetic acid, methanol (or ethanol) and methyl formate. Much lower intensity of peaks arising from carbon dioxide and –C–O– groups evolved during the thermal decomposition of POM/HAp composites can be observed from TG–FTIR results shown in Fig. 11, and normalized intensity of selected characteristic absorption bands is presented in Fig. 12.
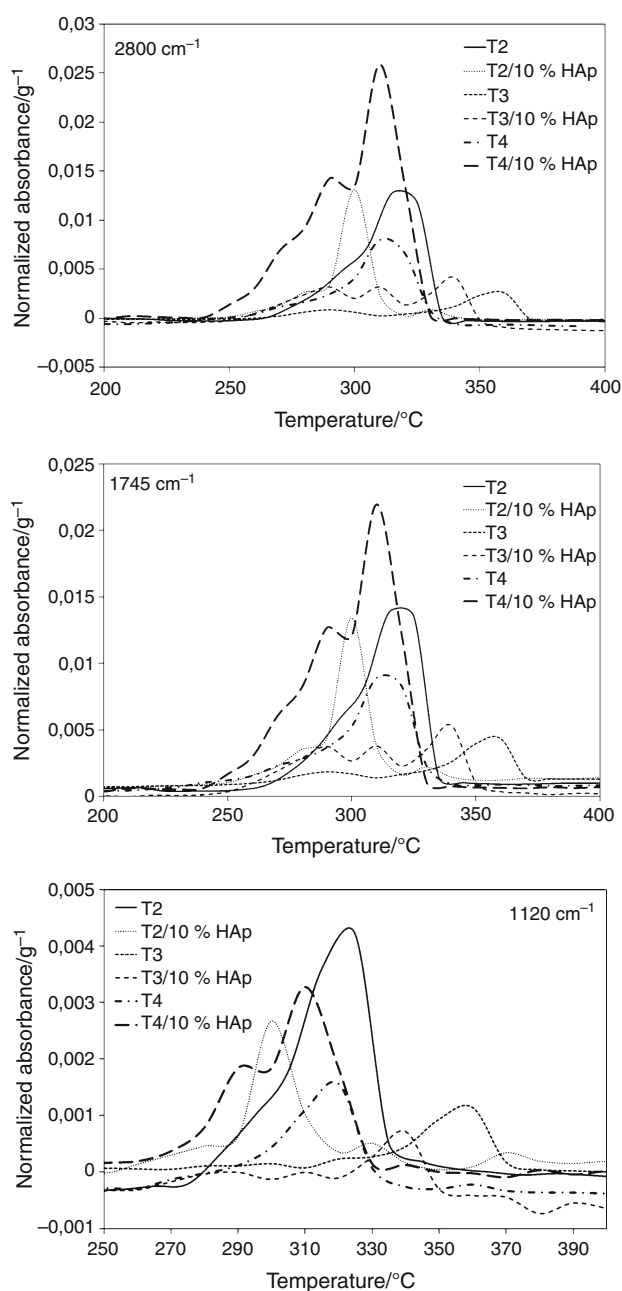
**Fig. 12** Normalized intensity of selected characteristic absorption bands of thermal degradation products of POM and POM/HAp nanocomposites

characteristic for compounds with –C–O– groups, was presented, too.

## Conclusions

The influence of mass-average molar mass of POM copolymers on the oxidative thermal degradation of POM-based nanocomposites with HAp was investigated. It was found that for pure POM copolymers thermal stability slightly decreases with a decrease in mass-average molar mass, while for POM/HAp nanocomposites the thermal stability of polymer matrix strongly depends on its molar mass. The lowest thermal stability was observed for nanocomposite with the lowest mass-average molar mass of POM. Kinetic analysis using Friedman and nonlinear regression methods revealed that degradation of pure POM copolymers runs through one main stage and that the starting reaction is autocatalytically activated. For POM/HAp nanocomposites with higher molar mass, the best fit was found for parallel autocatalytic and phase-boundary reaction model. Kinetics of decomposition of POM/HAp materials based on POM with the lowest molar mass included an additional parallel diffusion-controlled reaction. From thermoanalytical studies by hyphenated techniques, it was found that main degradation product for POM/HAp nanocomposites is formaldehyde and the amount of other degradation products was decreased in comparison with pure POM copolymers.

## References

1. Ramirez NV, Sanchez-Soto M, Illescas S. Enhancement of POM thermooxidation resistance through POSS nanoparticles. Polym Compos. 2011;32:1584–92.
2. Pielichowska K. Polyacetals. In: Olabisi O, Adewale K, editors. Handbook of Thermoplastics. 2nd ed. Boca Raton: CRC Press; 2015.
3. Lüftl S, Richaud E. Chemical resistance of polyoxymethylene. In: Luftl S, Visakh PM, Chandran S, editors. Polyoxymethylene handbook. London: Wiley; 2014. p. 277–99.
4. Yang F, Li H, Cai L, Lan F, Xiang M. Degradation and Stabilization of Co-POM. Polym-Plast Technol Eng. 2009;48:530–4.

For T2/10 % HAp, T3/10 % HAp and T4/10 % HAp, peaks corresponding to formaldehyde dominate. It confirms that in the presence of HAp reactions leading to formaldehyde formation are preferred. An important factor in oxidative degradation process of POM is its mass-average molar mass, too. As it can be seen from Fig. 12, the higher emission of formaldehyde (2800 and 1745 cm$^{-1}$) was detected for POM/HAp nanocomposites. In Fig. 12, the intensity of absorption band at 1120 cm$^{-1}$,

5. Luftl S, Archodoulaki VM, Seidler S. Thermal-oxidative induced degradation behaviour of polyoxymethylene (POM) copolymer detected by TGA/MS. Polym Degrad Stab. 2006;91:464–71.

6. Pan G, Li H, Cao Y. 1H-NMR investigation of the thermooxidation degradation of poly(oxymethylene) copolymers. J Appl Polym Sci. 2004;93:577–83.

7. Luftl S, Archodoulaki VM, Glantschnig M, Seidler S. Influence of coloration on initial material properties and on thermooxidative ageing of a polyoxymethylene copolymer. J Mater Sci. 2007;42:1351–9.

8. Kern W, Cherdron H, Jaacks V. Polyoxymethylene. Angew Chem. 1961;73:177–86.

9. Masamoto J. Modern polyacetals. Prog Polym Sci. 1993;18:1–84.

10. Kern VW, Cherdron H. Der abbau von polyoxymethylenen. Poloxymethylene. 14. Mitteilung. Makromol Chem. 1960;40:101–17.

11. Archodoulaki V-M, Koch T, Lüftl S, Seidler S, Stoiber R, editors. Correlation between molar mass and thermal/mechanical properties of polyoxymethylene (POM) copolymers. In: MoDeSt 2010, Athens, Greece.

12. Pielichowska K. The influence of molecular weight on the properties of polyacetal/hydroxyapatite nanocomposites. Part 2. In vitro assessment. J Polym Res. 2012;19:9788.

13. Zhang D, Zhao H, Zhao X, Liu Y, Chen H, Li X. Application of hydroxyapatite as catalyst and catalyst carrier. Prog Chem. 2011;23:687–94.

14. Sugiyama S, Moffat JB. The conversion of methanol: a probe reaction for hydroxyapatite. Catal Lett. 2001;76:75–80.

15. Matsumura Y, Moffat J. Catalytic oxidative coupling of methane over hydroxyapatite modified with lead. Catal Lett. 1993;17:197–204.

16. Pielichowska K, Blazewicz S. Bioactive polymer/hydroxyapatite (nano)composites for bone tissue regeneration. In: Abe A, Dusek K, Kobayashi S, editors. Biopolymers: lignin, proteins, bioactive nanocomposites. Adv Polym Sci. 2010;232:97–207.

17. Neumann M, Epple M. Composites of calcium phosphate and polymers as bone substitution materials. Eur J Trauma. 2006;32(2):125–31.

18. Pielichowska K. Thermooxidative degradation of polyoxymethylene homo- and copolymer nanocomposites with hydroxyapatite: kinetic and thermoanalytical study. Thermochim Acta. 2015;600:7–19.

19. Król P, Pielichowska K, Byczyński L. Thermal degradation kinetics of polyurethane–siloxane anionomers. Thermochim Acta. 2010;507–08:91–8.

20. Pielichowski K, Flejtuch K. Non-oxidative thermal degradation of poly(ethylene oxide): kinetic and thermoanalytical study. J Anal Appl Pyrol. 2005;73:131–8.

21. Vyazovkin S, Chrissafis K, Di Lorenzo ML, Koga N, Pijolat M, Roduit B, et al. ICTAC Kinetics Committee recommendations for collecting experimental thermal analysis data for kinetic computations. Thermochim Acta. 2014;590:1–23.

22. Vyazovkin S, Burnham AK, Criado JM, Pérez-Maqueda LA, Popescu C, Sbirrazzuoli N. ICTAC Kinetics Committee recommendations for performing kinetic computations on thermal analysis data. Thermochim Acta. 2011;520:1–19.

23. Opfermann J, Kaisersberger E. More information than activation energy from the model-free analysis according to Friedman, supplied with Netzsch Thermokinetics software.

24. Opfermann J, Kaisersberger E. An advantageous variant of the Ozawa–Flynn–Wall analysis. Thermochim Acta. 1992;203:167–75.

25. Khawam A, Flanagan DR. Solid-state kinetic models: basics and mathematical fundamentals. J Phys Chem B. 2006;110:17315–28.

26. Pielichowska K. The influence of molecular weight on the properties of polyacetal/hydroxyapatite nanocomposites. Part 1. Microstructural analysis and phase transition studies. J Polym Res. 2012;19:9775.

27. Hihara LH, Adler RPI, Latanision RM. Environmental degradation of advanced and traditional engineering materials. London: Taylor & Francis; 2013.

28. Tian M, Tan H, Li H, You C. Molecular weight dependence of structure and properties of chitosan oligomers. RSC Adv. 2015;5:69445–52.

29. Cordes HF. Preexponential factors for solid-state thermal decomposition. J Phys Chem. 1968;72:2185–9.

30. Sestak J. Thermophysical properties of solids, their measurements and theoretical thermal analysis. Amsterdam: Elsevier Science; 1984.

31. Pearson AWN, Groves GW. Thermal-degradation of polyoxymethylene produced by solid-state polymerization. J Polym Sci, Part B: Polym Phys. 1976;14:903–11.

32. Kumar G, Mahesh L, Neelakantan NR, Subramanian N. Studies on thermal-stability and behavior of polyacetal and thermoplastic polyurethane elastomer blends. Polym Int. 1993;31:283–9.

33. Sun TJ, Ye L, Zhao XW. Thermostabilising and nucleating effect of montmorillonite on polyoxymethylene. Plast Rubb Compos. 2007;36:350–9.

34. Jander W. Reaktionen im festen Zustande bei höheren Temperaturen. Reaktionsgeschwindigkeiten endotherm verlaufender Umsetzungen. Zeitschrift für anorganische und allgemeine. Chemie. 1927;163:1–30.

35. Ginstling A, Brounstein B. Concerning the diffusion kinetics of the reactions in spherical particles. J Appl Chem USSR. 1950;23:1327–38.

36. Duan YF, Li HL, Ye L, Liu XL. Study on the thermal degradation of polyoxymethylene by thermogravimetry-Fourier transform infrared spectroscopy (TG-FTIR). J Appl Polym Sci. 2006;99:3085–92.

37. Kern W. Chemische Elementarvorgänge bei der Alterungvon Kunststoffen. Chemiker-Ztg/Chem Apparatur. 1967;91:255–62.

38. Dudina LA, Yenikolopyan NS. Thermal and thermo-oxidative degradation of polyformaldehyde—II. Temperature dependence on the thermal degradation rate. Polym Sci USSR. 1964;5:36–45.

39. Sedlář VJ, Kučera M. Der thermooxydative abbau von polyformaldehyd. Makromol Chem. 1967;102(1):245–58.